An AC-DC converter with maximum power tracking for multi-input electromagentic energy harvester

Xianchao Liu
Min H. Kao Dept. of Electrical Engineering and Computer Science
The University of Tennessee, Knoxville
Knoxville,Tennessee
xliu125@vols.utk.edu

Han Peng
Huazhong University of Science and Technology
Wuhan, China
Pengh@hust.edu.cn

Leon M. Tolbert
Min H. Kao Dept. of Electrical Engineering and Computer Science
The Univversity of Tennessee
Knoxville, Tennessee
tolbert@utk.edu

2023 IEEE Energy Conversion Congress and Exposition (ECCE) | 979-8-3503-1644-5/23/$31.00 ©2023 IEEE | DOI: 10.1109/ECCE53617.2023.10362294

***Abstract*—Electromagnetic energy harvesters (EMEHs) have the potential to harvest various energy forms from different frequencies. But there is no AC-DC power converter that can achieve impedance matching for multi-input of a single energy harvester to extract maximum power from all frequency points. The article proposes a new AC-DC converter based on feedforward control to realize variable input impedance under different input frequencies. The article proposes an auxiliary coil to obtain the reference signal for feedforward control. The model of the auxiliary coil is built to guide the design. The AC-DC converter realizes variable impedance matching at different frequencies using an auxiliary coil. The article also analyzes the impedance mismatching loss caused by current ripple and builds a numerical calculation model. It can provide guidance for the design of key parameters, such as threshold voltage. The article designs a prototype of the AC-DC converter and EMEH with auxiliary coils. According to the measurement, the MPPT efficiency of the AC-DC converter is 98.7% at input frequency of 50 Hz and 97.7% at 1000 Hz. The converter transmission efficiency is 86.3%. The output voltage of AC-DC converter is 5 V with load resistor of 837 Ω. The overall of the multi-input energy harvesting system is 84.8%.**

Keywords—Multi-input, Energy harvesting, AC-DC converter, Impedance match, MPPT.

I. INTRODUCTION

With the popularity of wireless sensors, the self-powering problem of sensors has become a hot research topic. It is a premium power solution for equipment in extreme environments and situations which are not easy for battery exchange. Currently, energy harvesting is an efficient and alternative energy source to supply power for wireless sensors. In the power grid, there is a large amount of magnetic field energy. Therefore, the electromagnetic energy harvester (EMEH) is a good choice in the situation [1]-[6].

Magnetic field energy has different frequencies. Fig. 1 shows a photo of the measured 500kVA transformer in Guangxi, China and its magnetic flux density next to the output bus on the high voltage side at different frequencies. From the measurement result, it can be observed that there is a significant amount of magnetic field energy in the space, including power frequency, third harmonic, fifth harmonic, and other components. EMEHs have the potential to harvest EM energy from different frequencies. However, current micro-energy harvesting systems can only harvest energy with the same frequency. These single-source micro-energy harvesting systems consist of EMEH, an AC-DC converter, and an energy storage unit. The reliability and output power of these energy harvesting systems relying on a single energy source is low [6]. They are only suitable for some special applications where the power consumption is low. If power consumption is high, the output power of a single-source energy harvesting system is insufficient to support real-time operation of high-power sensors[7]-[12].

Therefore, in response to the higher power demands of applications and the complexity of environments, multi-input energy harvesting technology is needed.

Multi-input energy harvesting faces new challenges in maximum power point tracking (MPPT). Fig. 2 shows a multi-input energy harvesting system. The equivalent circuit model of an EMEH consists of a voltage source in series with a resistor

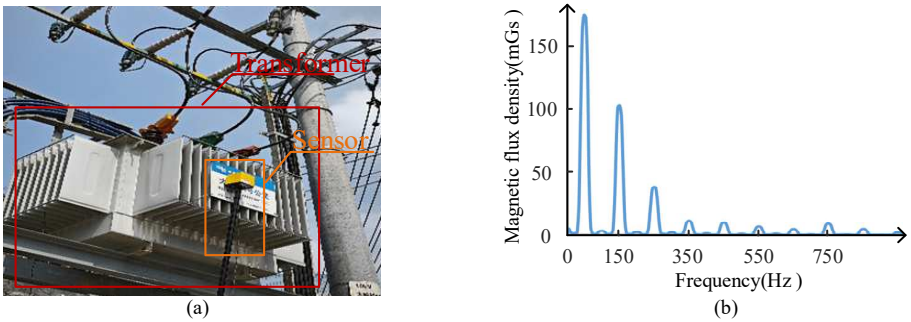

(a) (b)

Fig. 1. (a) The photo of the measured 500kVA transformer and (b) its magnetic flux density next to the output bus on the high voltage side at different frequencies.

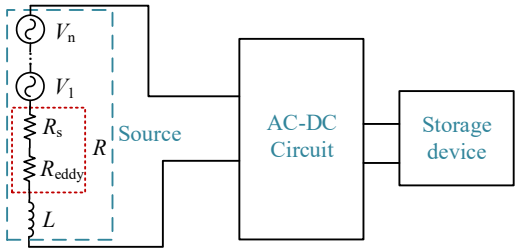

Fig. 2. Diagram of the multi-input EMEH system.

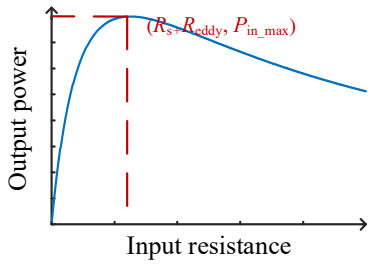

Fig. 3. Output power curve of EMEH when the reactance is matched.

and an inductor [13]. Therefore, the EMEH requires impedance matching through an AC-DC converter to achieve MPPT. The output power curve of EMEH is shown in Fig. 3. Maximum power can be extracted only when the device's reactance is matched and the output load is equal to the resistance.

However, the circuit's resistance includes coil resistance R_s and eddy current equivalent resistance R_{eddy}. R_{eddy} varies with frequency [14]. So, total equivalent resistance R and reactance vary with frequency. Therefore, it is necessary to achieve a variable input impedance at different frequencies of the AC-DC converter to achieve MPPT for multi-input EMEH.

This paper proposes an AC-DC converter using feedforward control strategy based on an auxiliary coil to achieve variable input impedance of the AC-DC converter to realize maximum power delivery for multi-input EMEH.

The organization of the rest of paper is as follows: Section II gives the theoretical modeling of an auxiliary coil and basic design of the AC-DC converter. Section III discusses the key design and simulation analysis of the AC-DC converter. The prototype of multi-input EMEH systems and related measurement results are provided in Section IV. Section V is the conclusions.

II. Control Strategy Based on Auxiliary Coil for AC-DC Converter

The topology of the AC-DC converter is shown in Fig. 4. The converter uses two NMOS device (M3, M4) and two PMOS device (M1, M2), which can decrease the complexity of the drive circuit. The converter uses the coil inductor as the switching inductor to decrease loss. To achieve impedance matching, it is necessary to control the input current of the converter, specifically the inductor current. Hysteresis control is adopted because it enables precise control of the inductor current, with high steady-state accuracy, fast response speed, and low implementation difficulty [13]. Fig. 5 shows the control schematic diagram of the AC-DC converter.

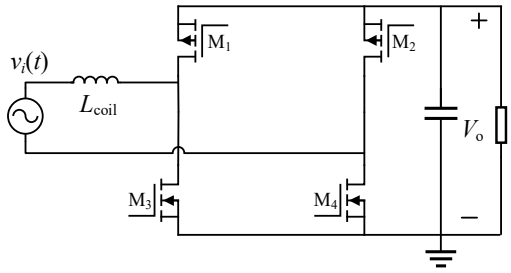

Fig. 4 Topology of the AC-DC converter.

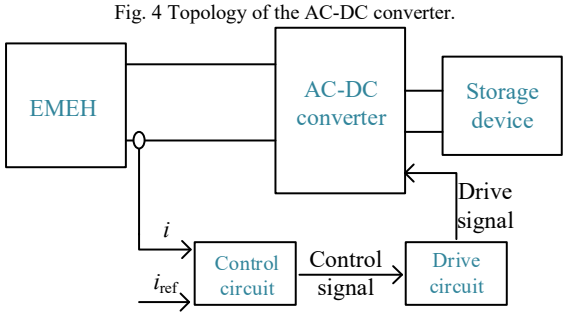

Fig. 5. Schematic diagram of EMEH system.

The control of the power devices is achieved by comparing the real-time inductor current with upper and lower threshold value of a reference current signal. When the inductor current operates in continuous conduction mode (CCM), the waveforms of the inductor current and the reference current are as shown in Fig. 6. i_{ref} is the current reference, and Δi is the current ripple threshold.

A. Feedback control based on auxiliary coil

As shown in Fig. 5, the key to current hysteresis control method is to generate a reliable and accurate current reference i_{ref}. Generally, i_{ref} is obtained by sampling the input voltage of EMEH and scaling it down proportionally [13]. However, when the coil inductance is used as the switching inductor, the curve of the input voltage will change to square wave. Ref. [13] proposed a method to obtain the induced electromotive force (EMF) reference of an EMEH using an auxiliary coil.

Fig. 7 shows an EMEH with auxiliary coil. The auxiliary coil cannot decrease the output power of the main coil [13]. Fig. 8 shows the coupled equivalent circuit model of an EMEH with auxiliary coil. v(t) is the EMF of the main coil. R_{eddy} is the eddy current equivalent resistance of the main coil, R_s is the resistance of the main coil, L_{coil} is the inductance of the main coil, R_{load} is the output resistance, $v_{EMF}(t)$ is the input voltage of the main coil, and $v_o(t)$ is output voltage of the main coil. $v_a(t)$ is EMF of the auxiliary coil, R_{eddy_aux} is the eddy current equivalent resistance of the auxiliary coil, R_{aux} is resistance of the auxiliary coil, L_{aux} is inductance of the auxiliary coil, R_{auxl} is equivalent input resistance of the sampling circuit, $v_{EMFaux}(t)$ is the input voltage of the auxiliary coil and $v_{aux}(t)$ is the open-circuit voltage of the auxiliary coil.

Defining the number of turns of the main coil is N_1, number of turns of the auxiliary coil is N_2, wire diameter of the coil is d_{wd}, μ_e is the relative magnetic permeability of the magnetic

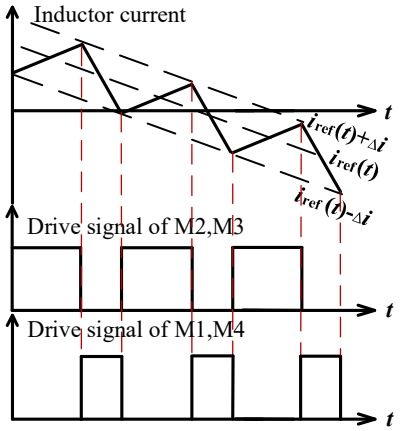

Fig. 6. Schematic diagram of current hysteresis loop control method.

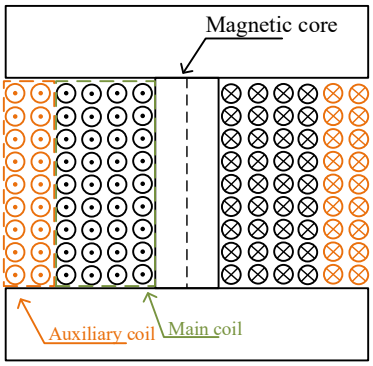

Fig. 7. Cross-section of a EMEH with auxiliary coil.

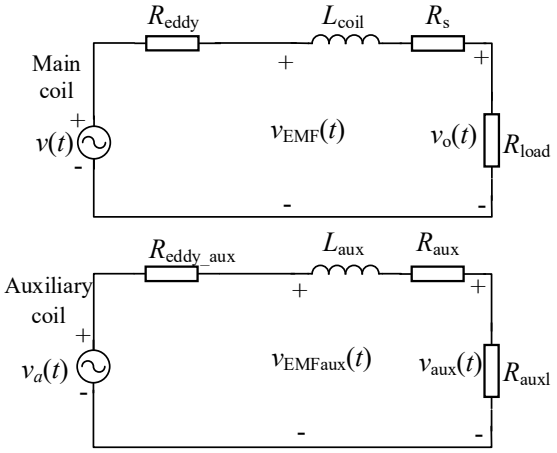

Fig. 8. Coupled equivalent circuit model of an EMEH with auxiliary coil.

core, and $B(t)$ is magnetic flux density in the cross-sectional area of the magnetic core.

Input voltage of the main coil, $v_{EMF}(t)$, is:

$$v_{EMF}(t)=\frac{\mu_e N_1 d_{wd}^{\ 2} B(t)}{4} \tag{1}$$

Input voltage of the auxiliary coil, $v_{EMFaux}(t)$, is:

$$v_{EMFaux}(t)=\frac{\mu_e N_2 d_{wd}^{\ 2} B(t)}{4} \tag{2}$$

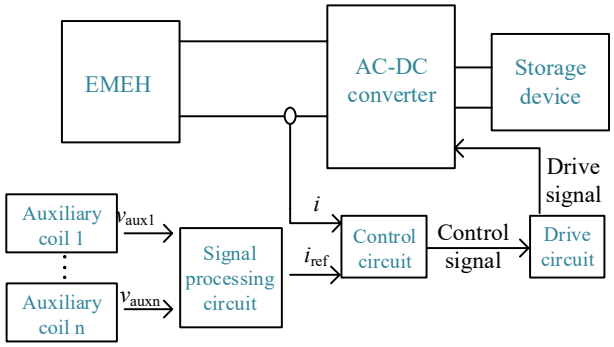

Fig. 9. Schematic diagram of multi-input EMEH system.

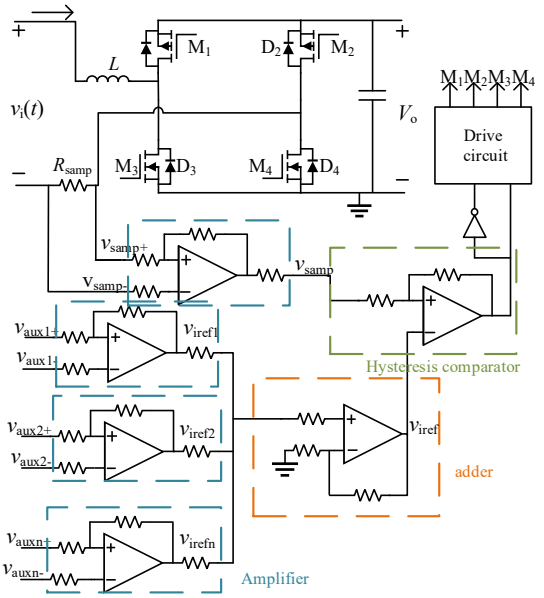

Fig. 10. Current hysteresis-loop control circuit based on auxiliary coil.

The current reference, $i_{ref}(t)$, is equal to the output current of the main coil when impedance matching is achieved. In this case, $R_{load} = R_s + R_{eddy}$ and L_{coil} is matched. $i_{ref}(t)$ is expressed as:

$$i_{ref}(t)=\frac{v_{EMF}(t)}{2R_s+R_{eddy}}=\frac{N_1}{N_2(2R_s+R_{eddy})}v_{EMFaux}(t) \tag{3}$$

Generally, output of the auxiliary coil is connected to input characteristic of the sampling circuit, where R_{auxl} is greater than 100 kΩ. Therefore, $v_{aux}(t)$ is approximately equal to $v_{EMFaux}(t)$. By sampling the output voltage of the auxiliary coil, $v_{aux}(t)$, and then amplifying it by a factor of $N_1 / (N_2(2R_s + R_{eddy}))$, the current reference, $i_{ref}(t)$, can be obtained.

B. Impedance matching for multi-input EMEH

The above section introduced the current hysteresis loop control method for EMEH based on auxiliary coil. By using an auxiliary coil, the current reference for different frequencies can be obtained for EMEH to achieve impedance matching for multi-input sources. As shown in Fig. 9, the current hysteresis loop control method based on this auxiliary coil primarily

consists of the auxiliary coils, a signal processing circuit, and a control circuit including hysteresis comparator. The current hysteresis-loop control circuit based on the auxiliary coil is shown as Fig. 10.

Output voltage and phase of the auxiliary coil for the n_{th} source are obtained by sampling through the n_{th} auxiliary coil; it is expressed as:

$$v_{auxn}(t) = V_{auxn}\sin(2\pi f_n t + \theta_n) \tag{4}$$

V_{auxn} is voltage amplitude of the n_{th} auxiliary coil, f_n is frequency, and θ_n is phase of the voltage. By amplifying V_{auxn}, $v_{irefn}(t)$ is obtained:

$$v_{irefn}(t) = V_{irefn}\sin(2\pi f_n t + \theta_n) \tag{5}$$

To obtain $i_{iref}(t)$, $v_{iref1}(t)$, $v_{iref2}(t)$, ..., $v_{irefn}(t)$ are scaled down by different factors and then summed together.

The inductor current will fluctuate within the range of $i_{ref}(t)$-Δi to $i_{ref}(t)$+Δi, where Δi is the maximum value of the current ripple. Δi is controlled by threshold voltage of the hysteresis comparator ΔU_d.

By neglecting the current ripple, the output power of EMEH P_{outE} can be further expressed as:

$$P_{outE} = \sum_{i=1}^{n} \frac{V_i^2}{8(R_{eddy\_i} + R_{s\_i})} \tag{6}$$

where V_n is open-circuit voltage amplitude of the n_{th} source.

According to (6), when the AC-DC converter achieves variable input impedance under different frequencies, the input power of the AC-DC converter is equal to the sum of the maximum output power of each source of multi-input EMEH when impedance matching is achieved.

III. Threshold Voltage Design

In the current hysteresis loop control method, as the threshold voltage ΔU_d of the hysteresis comparator increases, the switching frequency of the AC-DC converter decreases, resulting in lower switching loss. However, a higher threshold voltage ΔU_d leads to increased current ripple, resulting in impedance mismatching and lower theoretical maximum extraction efficiency of the AC-DC converter. Therefore, the threshold voltage is a key parameter in the design of current hysteresis loop control circuit.

A. Theoretical model of switching loss and impedance mismatching loss

In order to analyze the relationship between the threshold voltage and the switching loss of the converter, as well as the loss caused by impedance mismatching due to current ripple, it is necessary to derive formulas between the threshold voltage ΔU_d and the switching frequency f_s. However, the switching frequency will vary with the input voltage as shown in Fig. 11. To simplify the analysis, the average switching frequency f_{sa} is defined as [15]:

$$f_{sa} = \frac{R_{samp}k(2V_oV_p - V_p^2)}{2L_{coil}V_o\Delta U_d} \tag{7}$$

where R_{samp} is resistance of sampling in the power circuit, k is amplification ratio of the sampled voltage, V_p is voltage amplitude of the source under one frequency and V_o is output voltage of the converter.

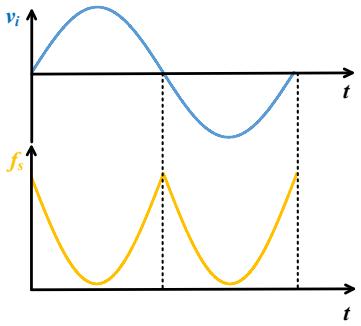

Fig. 11. Curve of switching frequency and input voltage of the converter.

The switching loss of the circuit mainly consists of turn-on loss, turn-off loss, and loss caused by the discharge of the output capacitance of power devices during switching [15]. The expression for these losses can be expressed as:

$$P_{loss} = 2P_{loss\_swN} + 2P_{loss\_swP} + 2P_{lossN\_c} + 2P_{lossP\_c} \tag{8}$$

P_{loss_swN} is the turn-on and turn-off loss of the NMOS, while P_{loss_swP} is the turn-on and turn-off loss of the PMOS. P_{lossN_c} and P_{lossP_c} are the losses generated by the discharge of the output capacitances of the NMOS and PMOS during switching. P_{loss_sw} can be expressed as:

$$P_{loss\_sw} = \frac{1}{2}\frac{1}{T_i}\sum_N E_{offk} = \frac{V_oV_pf_{sa}(t_{off} + t_{on})}{16\pi} \tag{9}$$

where T_i is a switching cycle. t_{off} and t_{on} is turn-on and turn-off time of the switches.

So, P_{loss_sw} can be calculated as:

$$\begin{aligned} P_{loss\_sw} &= \frac{V_o^2(C_{oss\_N} + C_{oss\_P})R_{samp}k(2V_oV_p - V_p^2)}{32L_{coil}V_o\Delta U_d} \\ &+ \frac{V_oV_pR_{samp}k(t_{off\_N} + t_{on\_N} + t_{off\_P} + t_{on\_P})(2V_oV_p - V_p^2)}{16\pi L_{coil}V_o\Delta U_d} \end{aligned} \tag{10}$$

Similarly, P_{loss_c} can be expressed as:

$$P_{loss\_c} = \frac{V_o^2C_{oss}R_{samp}k(2V_oV_p - V_p^2)}{64L_{coil}V_o\Delta U_d} \tag{11}$$

According to (10) and (11), the switching loss P_{loss} can be calculated.

The calculation for impedance mismatching loss caused by current ripple is given as follows. Considering the current ripple, the input power of one switching cycle, $P_{in\_avg}(t)$, is:

$$P_{in\_avg}(t) = \frac{v_i(t)^2}{4R} - \frac{2R(v_i(t) + V_o)(\Delta i)^2}{3(V_o - v_i(t))} \tag{12}$$

Therefore, the theoretical maximum input power for one AC cycle, P_{in_max}, is:

$$P_{in\_max}(t) = \frac{V_p^2}{8R} - \frac{R\Delta i^2}{3\pi fN}\sum_0^{N_i} \frac{(V_p\sin(2\pi\frac{N}{N_i}) + V_o)}{(V_o - V_p\sin(2\pi\frac{N}{N_i}))} \tag{13}$$

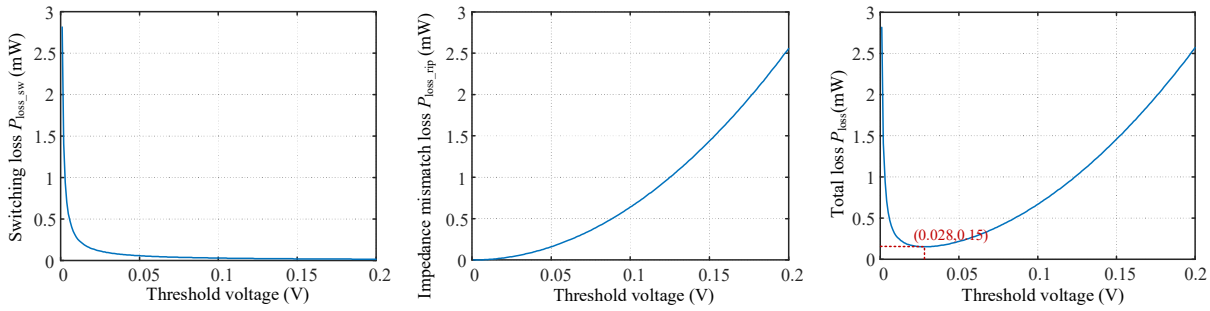

Fig. 12. Curve of (a) switching loss, (b)impedance mismatching loss, (c) total loss under different threshold voltage.

The loss caused by impedance mismatching due to current ripple, P_{loss_rip}, is:

$$P_{loss\_rip} = \frac{R_{in}\Delta U_d{}^2}{3\pi f N R_{samp}{}^2 k^2} \sum_{0}^{N_i} \frac{(V_p \sin(2\pi \frac{N}{N_i}) + V_o)}{(V_o - V_p \sin(2\pi \frac{N}{N_i}))} \quad (14)$$

By combining (10), (11) and (14), the relationship between the total loss of the circuit, P_{loss}, and the threshold voltage, ΔU_d, can be obtained:

$$P_{loss} = P_{loss\_rip} + P_{loss\_sw} \quad (15)$$

To calculate the total loss, the parameters of the switching devices are required. In this paper, the selection method from [15] is used to choose the power devices. Specifically, an GaN-HEMT EPC2037 and a PMOS PMV160 are selected. The device parameters are shown in TABLE I. The switching loss at different threshold voltages is shown in Fig. 12(a). As the threshold voltage increases, the switching loss gradually decreases.

To calculate the impedance mismatching loss, the theoretical maximum output power and the equivalent resistance of EMEH is required. Assume that the theoretical maximum output power of the EMEH is 20 mW and the equivalent resistance is 50 Ω. The actual resistance mismatching loss at different threshold voltages is shown in Fig. 12(b). As the threshold voltage increases, the impedance mismatching increases, but the rate of increase becomes slower.

The total circuit loss P_{loss} at different threshold voltages is shown in Fig. 12(c). The total loss initially decreases and then increases as the threshold voltage increases. The minimum P_{loss} is 0.15 mW at a threshold voltage of 28 mV.

Therefore, 28 mV is chosen as the threshold voltage design value to minimize the total loss. The average switching frequency f_{sa} is 103 kHz.

IV. Experimental Prototype

As shown in Fig. 13, the prototype of the AC-DC converter is fabricated. The size of the circuit is 3.5 cm x 4.8 cm. The key components of the converter are shown in TABLE II. All components are low-power devices. As shown in Fig. 14, the prototype of an EMEH with auxiliary coils is fabricated. The volume of the device is 49 cm^3, and the magnetic core material is manganese-zinc ferrite with a relative magnetic permeability of 2000. Key parameters of the EMEH are shown in TABLE III.

To simulate the magnetic field environment, a magnetic field energy generation platform is constructed as shown in Fig. 15.

TABLE I. Key Parameters of the Switches

Part number	t_{on}	t_{off}	C_{oss}	R_{ds_on}	Q_g
EPC2037	0.48ns	0.67ns	420pF	400mΩ	115pC
PMV160	1ns	0.5ns	42pF	210mΩ	3.3nC

TABLE II. Key Parameters of the AC-DC Converter

Device	Part number
Switches	EPC2037 PMV160
Analog amplifier	LTC6078 LTC6255
Comparator	TLV7011
Supply	TPS78101

TABLE III. Key Parameters of the EMEH

Coil	Number of turns	Resistance	Inductance
Main coil	1500	38.5 Ω	390 mH
Auxiliary coil	200	3.5 Ω	20 mH

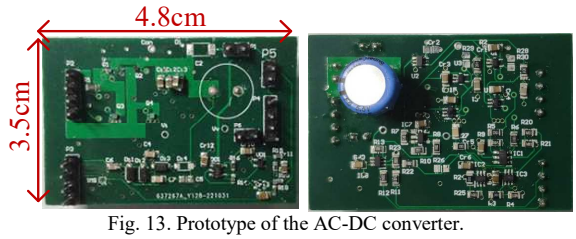

Fig. 13. Prototype of the AC-DC converter.

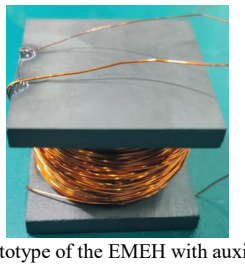

Fig. 14. Prototype of the EMEH with auxiliary coils.

The platform consists of signal generator, power amplifier, oscilloscope, and Helmholtz coil. The Helmholtz coil can generate a uniform magnetic field. The photo of the platform is shown in Fig. 16.

A. Prototype of EMEH with auxiliary coil and test bench

Before experiments on the multi-input energy harvesting system, it is necessary to test the EMEH to obtain its output characteristics.

Fig. 17 shows the input voltage waveforms of the prototype of the EMEH in a 50 Hz / 7.6 Gs magnetic field. The black waveform is the input voltage $v_{EMF}(t)$ of the main coil, while the blue waveform is the input voltage $v_{EMFaux}(t)$ of the auxiliary coil. Voltage frequencies of the auxiliary coil and the main coil

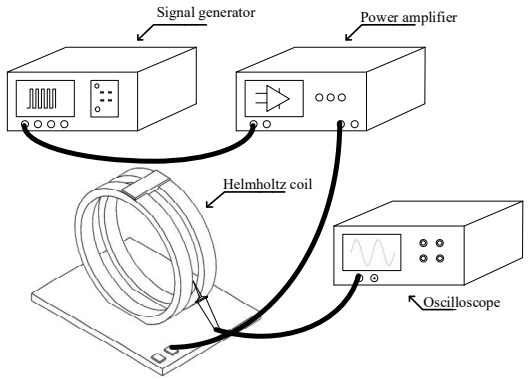

Fig. 15. Diagram of magnetic field generation platform.

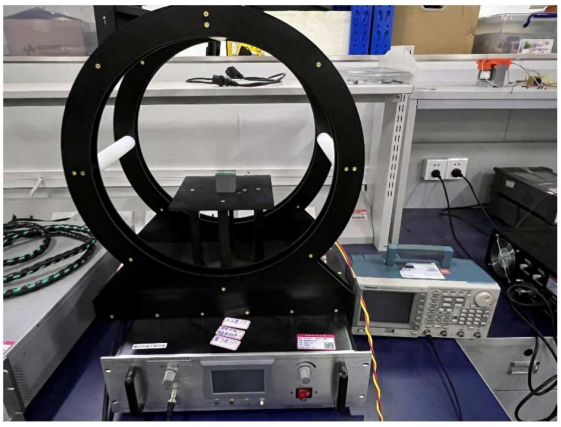

Fig. 16. Photo of magnetic field generation platform.

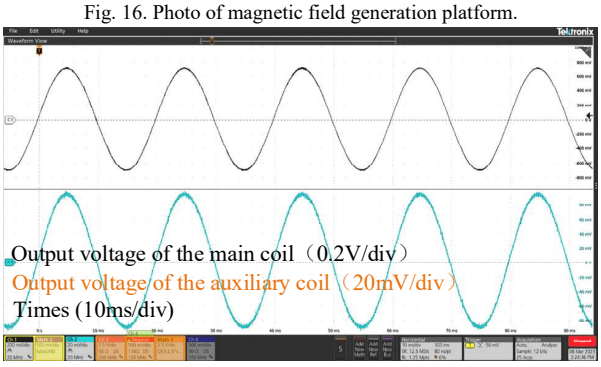

Fig. 17. Input voltage waveforms of prototype of the EMEH in a 50 Hz / 7.6 Gs magnetic field.

are the same, both at 50 Hz, with a phase difference of 0. Voltage amplitude of the main coil is 720 mV, and voltage amplitude of the auxiliary coil is 95mV. The amplitude ratio is approximately 7.57, which is approximately equal to the turn ratio of 1500/200=7.5. Therefore, input voltage signal of the auxiliary coil can be used to obtain the phase and amplitude of the input voltage of the main coil.

Magnetic field generation platform generates 50 Hz magnetic field to simulate energy from power grid and 1000 Hz magnetic field to simulate energy from power electronics. Fig. 18 shows the output voltage curve and output power curve of the EMEH in the given magnetic field environment. The prototype achieves its maximum output at an output load of 80 Ω, which is 17.92 mW under 50 Hz / 7.6 Gs magnetic field. The prototype achieves its maximum output at an output load of 120 Ω, which is 17.28 mW under 1000 Hz / 400 mGs magnetic field.

B. Experiment for multi-input EMEH system

This section verifies the operation of the multi-input EMEH system. Magnetic field generation platform generates a mixed magnetic field with 50 Hz / 7.6 Gs and 1000 Hz / 400 mGs.

The hysteresis control function of the AC-DC converter is verified. The waveforms of inductor current and drive voltage are shown in Fig. 19. Fig. 20 shows the input voltage waveform of the AC-DC converter. TABLE IV summarizes key parameters of the AC-DC converter. The RMS of the input current of the AC-DC circuit is 18.96 mA including 14.64 mA at 50 Hz and 12.06 mA at 1000 Hz. The RMS of input voltage of the AC-DC converter is 1.865 V including 1.21 V at 50 Hz and 1.4 V at 1000 Hz. Therefore, the input power at 50 Hz for

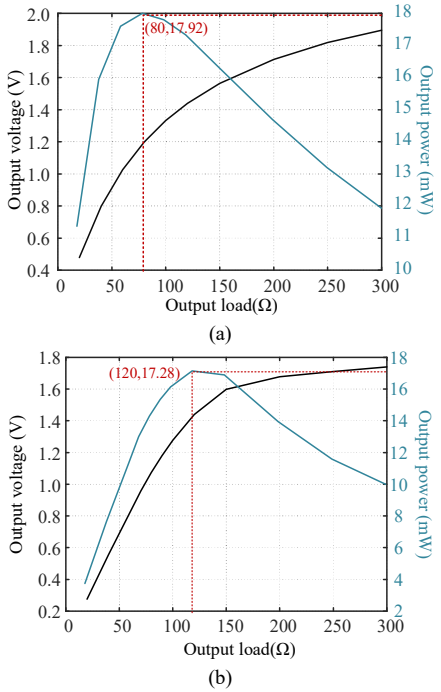

Fig. 18 Output voltage curve and output power curve of the EMEH in the given magnetic field environment (a) 50Hz/7.6Gs (b) 1000Hz/400mGs.

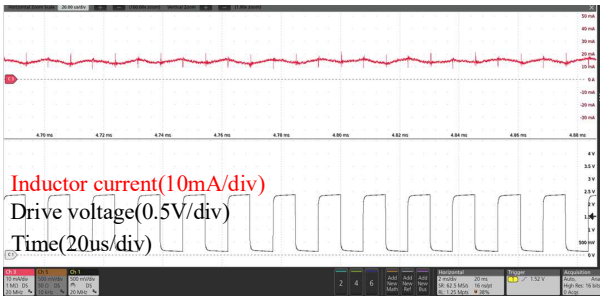

Fig. 19 Waveforms of inductor current and drive voltage.

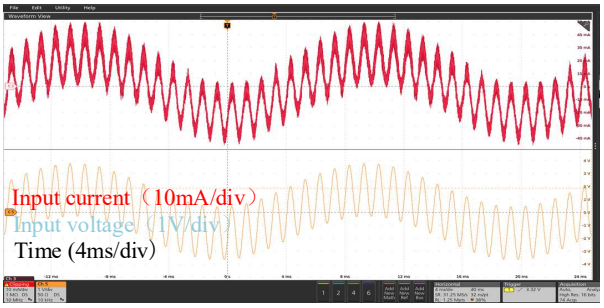

Fig. 20 Input voltage waveform of the AC-DC converter.

the AC-DC circuit is 17.71 mW, and at 1000 Hz is 16.88 mW. So the overall input power is 34.59 mW. Thus, the converter achieves 17.71/17.92 mW=98.7% MPPT efficiency for 50 Hz magnetic field and 16.88/17.28 mW=97.68% MPPT efficency for 1000 Hz magnetic field. TABLE V summarizes output parameters of the system. Output of the AC-DC converter is 5 V / 837 Ω with an output power of 29.86 mW. The converter transmission efficiency is 29.86 mW / (17.71+16.88) mW =86.3%. The overall efficiency of the system is 29.86 mW / 35.2 mW = 84.8%.

V. CONCLUSIONS

This paper proposes an impedance matching strategy for multi-input EMEH systems based on an auxiliary coil. The theoretical model of the auxiliary coil is proposed to guide the design of the control circuit. Considering the impact of current ripple on impedance mismatching, theoretical guidance is provided for the design of the threshold voltage of the hysteresis control circuit. Finally, a prototype of EMEH with an auxiliary coil and AC-DC converter is developed, and a prototype of the multi-input EMEH system is built. Experimental results demonstrate that under a mixed magnetic field with input sources at 50 Hz and 1000Hz, the system successfully achieves 97.8% MPPT efficiency for the 50 Hz magnetic field and 98.7% MPPT efficiency for the 1000 Hz magnetic field. The total output power of the system is 29.86 mW with a total efficiency of 84.8%.

TABLE IV. KEY PARAMETERS OF THE INPUT FOR THE AC-DC CONVERTER

Frequency	Input voltage	Input current	Input power	Maximum input power	MPPT efficiency
50 Hz	1.21 V	14.64 mA	17.71 mW	17.92 mW	98.70%
1000 Hz	1.4 V	12.06 mA	16.88 mW	17.2 8mW	97.68%

TABLE V. OUTPUT PARAMETERS OF THE SYSTEM

Output voltage	Output power	Transmission efficiency	Overall efficiency
5 V	29.86 mW	86.3%	84.8%

REFERENCES

[1] S. Wang, Y. Ke, P. Huang and P. Hsieh, “Electromagnetic energy harvester interface design for wearable applications,” *IEEE Transactions on Circuits and Systems II: Express Briefs*, 2018, vol. 65, no. 5, pp. 667-671.

[2] M. Rossi, S. Member, L. Rizzon, M. Fait, R. Passerone and D. Brunelli, “Energy neutral wireless sensing for server farms monitoring,” *IEEE Journal on Emerging and Selected Topics in Circuits and Systems*, 2014, vol. 4, no. 3, pp. 324-334.

[3] R. Vullers, R. Schaijk, H. Visser, J. Penders, and C. Hoof, “Energy harvesting for autonomous wireless sensor networks,” *IEEE Solid-State Circuits Magazine*, 2010, vol. 2, no. 2, pp. 29-38.

[4] G. Giaconi, D. Gündüz, and H. V. Poor, “Smart meter privacy with renewable energy and an energy storage device,” *IEEE Transaction on Information Forensics and Security*, 2018, vol. 13, no. 1, pp. 129-142.

[5] S. P. Pellegrini, N. Tolou, M. Schenk, and J. L. Herder, “Bistable vibration energy harvesters: A review,” *J. Intell. Mater. Syst. Struct.*, 2012, vol. 24, no. 11, pp. 1303-1312.

[6] Y. Yang, T. Cai, S. Xue, X. Song, and X. Cui, “High performance hybrid piezoelectric-electromagnetic energy harvester for scavenging energy from low-frequency vibration excitation,” *IEEE Access*, 2020, vol. 8, pp. 206503-206513.

[7] D. Ma, G. Lan, M. Hassan, W. Hu and S. K. Das, “Sensing, computing, and communications for energy harvesting IoTs: a survey,” *IEEE Communications Surveys & Tutorials*, 2020, vol. 22, no. 2, pp. 1222-1250.

[8] A. Bibo and M. F. Daqaq, “Investigation of concurrent energy harvesting from ambient vibrations and wind ,” *Physics Letters*, 2013, vol. 102, no. 24, pp. 243804.

[9] R. C. Vinod, “Vibration energy harvesting for low power and wireless applications,” Ph.D. Dissertation, Stevens Institute of Technology, Hoboken, NJ, 2010.

[10] P. K. Sharma, J. Park, J. H. Park and K. Cho, “Wearable computing for defence automation: opportunities and challenges in 5G network,” *IEEE Access,* 2020, vol. 8, pp. 65993-66002.

[11] L. Sigrist, N. Stricker, D. Bernath, J. Beutel and L. Thiele. Thermoelectric energy harvesting from gradients in the earth surface. *IEEE Transaction on Industrial Electronics*, 2020, vol. 67, no. 11, pp. 9460-9470.

[12] V. Nico, R. Frizzell and J. Punch, “The identification of period doubling in a nonlinear two-degree-of-freedom electro-magnetic vibrational energy harvester,” *IEEE Transactions on Mechatronics*, 2020, vol. 25, no. 6, pp. 2973-2980.

[13] H. Xiao, H. Peng, X. Liu and H. Sun, “Fully Self-Powered Inductor-Less Electromagnetic Vibration Energy Harvesting System Using Auxiliary Coils for Hysteresis Current MPPT Control,” *IEEE Transactions on Power Electronics*, 2022, vol. 37, no. 11, pp. 13192-13204.

[14] S. B. Shah, P. Rasilo, A. Belahcen and A. Arkkio, “Experimental and theoretical study of interlaminar eddy current loss in laminated cores," 2017 20th International Conference on Electrical Machines and Systems (ICEMS), Sydney, NSW, Australia, 2017.

[15] J. Chen, H. Peng, Z. Feng, Y. Kang, “A GaN BCM AC–DC converter for sub-1 V electromagnetic energy harvesting with enhanced output power,” *IEEE Transactions on Power Electronics*, 2021, vol. 36, no. 8, pp. 9285-9299.